Identification of the "Voided Double-Gyroid-Channel": A New Morphology in Block Copolymers

Takeji Hashimoto,*,†,‡,§ Yukihiro Nishikawa⊥,† and Kiyoharu Tsutsumi†,#

Hashimoto Polymer Phasing Project, ERATO, JST, Japan, and Department of Polymer Chemistry, Graduate School of Engineering, Kyoto University, Katura, Nishikyo-ku, Kyoto 615-8510, Japan

Received August 1, 2006; Revised Manuscript Received November 30, 2006

ABSTRACT: We unequivocally verified a success of creating "voided double-gyroid-channel" morphology and identified for the first time its cleavage planes inherent in the morphology on the basis of computer analysis of field-emission scanning electron microscope (FE-SEM) images. This morphology was created by transforming the minor network phase of the double-gyroid cubic structure of block copolymers with $Ia\bar{3}d$ space group symmetry into empty space. The fabrication process leading to the morphology was proven to conserve the original double-gyroid structure. The FE-SEM images observed on the freeze-fractured surface of the morphology exhibited almost only two kinds of patterns: "periodic double-wave pattern" and "hexagonal doughnut pattern". Thus, the images observed on the freeze-fractured surfaces are "deterministic", compared with those observed under transmission electron microscopy on the ultrathin-sectioned specimens which essentially vary randomly, depending on the sectioning directions relative to the cubic structure. These unique patterns were identified to appear respectively on the cleavage planes parallel to (211) plane and (110) plane of the cubic structure on which the cross-sectional area of the morphology becomes minimal. These patterns together with facets, which appear at the places where the successive cleavage planes with a characteristic step-height difference merge together, unveiled unequivocal pieces of evidence for conservation of the cubic structure before and after the fabrication process and hence for creation of the unique morphology potentially important for nanotechnology. They also elucidate basic information on a fracture mechanism of the unique morphology.

I. Introduction

The double-gyroid network structure with $Ia\bar{3}d$ space group symmetry is a unique but universal structure found in various systems[1] such as block copolymers,[2] ordered mesoporous silica,[3] surfactant systems,[4] lipids,[5] etc. Bates and co-workers identified the location of the gyroid phase in the phase diagram of a block copolymer.[6] They have been characterized by transmission electron microscopy (TEM),[7] TEM with electron tomography,[8] small-angle X-ray scattering (SAXS),[9] small-angle neutron scattering (SANS),[10] and the electron crystallography method.[3] The structure is unique in that both the network phase and its matrix phase are continuous in three-dimensional (3D) space and hence attracts interests of many researchers toward nanoscience and nanotechnology.

As the road forward nanotechnology, we for the first time reported a fabrication of the double-gyroid network structure to create the so-called "voided double-gyroid-channel" structure in a short communication in 1999.[11] The fabrication involved a selective chemical degradation of the minor network phase of the double-gyroid structure in order to transform the phase into the vacant channel phase without significant perturbations of the ordered structure and the $Ia\bar{3}d$ space group symmetry. The new morphology thus created was further fabricated to load metal nanoparticles on the interface between the vacant channel phase and the matrix phase for a possible application as a membrane reactor.

The new morphology as described above is quite novel, interesting, and potentially important for nanotechnology and science because it contains an ordered, vacant channel of nanosized cross section, which is continuous in 3D space, in the glassy polymer matrix. However, the characterization of the new morphology and verification or identification of it was still far from complete. Therefore, since 1999 we have collected many FE-SEM images and made an extensive computer analysis of the images. In this work we aim to unequivocally verify a success in creating the new morphology having essentially the same long-range order and symmetry as the original double-gyroid morphology. Since 1999 up to present, there have been no other reports for a success of creating the new morphology, "voided double-gyroid-channel morphology"; we believe the work is worthy of being reported at this stage.

In the course of the work, we encountered such a new piece of evidence that the images observed under field-emission scanning electron microscopy (FE-SEM) on the freeze-fractured surfaces of the fabricated materials exhibit almost only two kinds of patterns—the "periodic double-wave pattern" as reported earlier[11] and the newly found "hexagonal doughnut pattern" to be reported in this paper—both of which are accompanied by facets. We believe that explorations of physical significances of the above piece of evidence would be an important not only from the viewpoint of nanoscience and technology but also from the viewpoint of micromechanics of the unique structure. Elucidation of this evidence is another important aim of this work.

* To whom correspondence should be addressed.
† Hashimoto Polymer Phasing Project, ERATO, JST.
‡ Kyoto University.
§ Present address: Advanced Science Research Center, Japan Atomic Energy Agency, Tokai, Ibaraki 319-1195, Japan.
⊥ Present address: Department of Polymer Science and Engineering, Kyoto Institute of Technology, Matsugasaki, Sakyo-ku, Kyoto 606-8585, Japan.
Present address: Research Center, Daicel Chemical Industries, Ltd., 1239, Shinzaike, Aboshi-ku, Himeji, Hyogo 671-1283, Japan.

10.1021/ma061739h CCC: $37.00
Published on Web 01/26/2007

Table 1. Characterization of Polymers Used in This Work

polymer[a]	$M_w \times 10^{-4}$	$M_n \times 10^{-4}$	w_I
SI	9.1	8.8	0.49
VI	14.7	12.8	0.27
HS	0.79	0.75	0
HI	0.42	0.40	1

[a] SI = polystyrene-*block*-polyisoprene, VI = poly(2-vinylpyridine)-*block*-polysioprene, HS = homopolystyrene, and HI = homopolyisoprene.

Therefore, in this work we focus on further analyses of the patterns and facets that appeared on the FE-SEM images for the materials, which was previously suggested to seemingly have the voided double-gyroid-channel morphology, with an aid of computer analysis based on an approximate equation in differential geometry[1] for the double-gyroid network. We shall extend our previous observation on film specimens of polystyrene-*block*-polyisoprene (SI) mixed with homopolystyrene (HS) (SI/HS mixture) to another system of poly(2-vinylpyridine)-*block*-polyisoprene (VI) mixed with homopolyisoprene (HI) as well with an aim to generalize our observation. We shall identify that the two patterns observed on fracture surfaces reveal the most common cleavage planes of the voided double-gyroid structure and further elucidate that the facets are observed at places where the two successive cleavage planes with the characteristic step-height difference merge together. The two patterns with the characteristic facets will be important also for unequivocal verification of creation of the voided double-gyroid-channel morphology with $Ia\bar{3}d$ space group symmetry.

II. Experimental Section

II-1. Polymer Samples and Film Specimens. The same polymers and film specimens as those previously reported[11] were used for the SI/HS specimens with total volume fraction of polyisoprene (PI) 0.34, the details of which should be referred to the previous report. The VI block copolymers newly used in this study were synthesized as described elsewhere.[12] They were mixed with HI in such a way that volume fraction of PI becomes 0.4. The characteristics of the polymers used in this work are summarized in Table 1. The mixture of VI/HI was dissolved into solution of ca. 5 wt % total polymer concentration solution with chloroform. Then films about 100−300 μm thick were prepared by slowly evaporating solvent over ca. 1 week. The as-cast films were further dried until a constant weight was attained.

II-2. Selective Cross-Linking of Matrix Phase. Before applying the selective degradation to the PI network phase, the P2VP matrix phase of VI/HI was subjected to a selective cross-linking, while the PS matrix phase of SI/HS was not subjected to the selective cross-linking. To cross-link the P2VP matrix phase, the VI/HI films were exposed to 1,4-diiodobutane (DIB) vapor for 24 h at 80 °C, followed by drying for 48 h under vacuum.[13] The cross-linking was found to stain selectively the P2VP microphase, giving rise to dark contrast for the P2VP microphase and bright contrast for the PI microphase under TEM and changed the film from transparent to a yellowish appearance.

II-3. Selective Degradation with Ozonolysis. Lee et al.[14] already reported the selective degradation of PI domain with ozonolysis. We followed essentially the same procedure as that employed by Lee et al. and as detailed in our previous publication.[11] To cleave the carbon−carbon double bond of PI constituting the double network phase in the matrix of the cross-linked P2VP phase or un-cross-linked PS phase, the films were exposed to an atmosphere of ozone for 24 h at room temperature. The cleaved compounds were leached out from the network phase by soaking the film in ethanol for 24 h at room temperature. The extent of PI removal was ca. 100% for the film having thickness of ca. 100 μm, which was determined from an NMR measurement and a weight measured before and after ozonolysis.

II.4. Electron Microscopy. Morphology of the film specimens before the ozonolysis was studied under transmission electron microscopy (TEM) on ultrathin sections stained with O_SO_4 or DIB vapor. For this purpose a JEOL JEM-2000FXZ operated at 160 kV and a Reichert-Nissei Ultracut-S ultramicrotome were used. Morphology of the film specimens after the ozonolysis was studied under a scanning electron microscopy with a field-emission gun (FE-SEM) on freeze-fractured surfaces. For this purpose Hitachi S-900S operated at 20 kV was used. The freeze-fractured surfaces, obtained according to a conventional method, were sputter-coated with platinum by using Hitachi E-1030 ion sputter for FE-SEM observation.

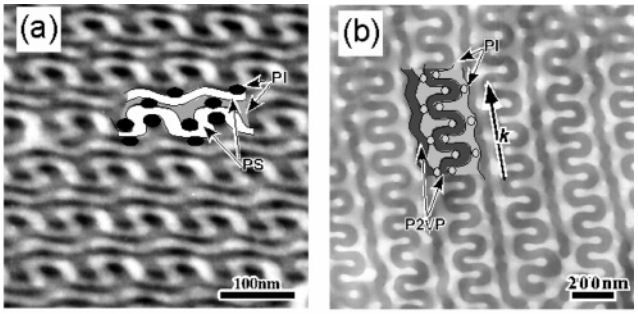

Figure 1. TEM images of ultrathin sections of the SI/HS films stained with O_SO_4 vapor (a) and VI/HI films stained with 1,4-diidobutane (b). The inset shows a schematic of the double-wave pattern.

III. Results

III-1. Morphological Characterization of Specimens before Ozonolysis. Figure 1 represents a TEM image for ultrathin section of the SI/HS films (un-cross-linked) stained with O_SO_4 (part a) and that for ultrathin sections of VI/HI films cross-linked with DIB (part b) but unstained with O_SO_4. In part a for the SI/HS films, the minority phase of PI was stained dark and gray with O_SO_4 and the unstained majority phase of PS appears bright, while in part b for the VI/HI films, the majority or matrix phase was stained dark with DIB, but the unstained PI network phase appears to be bright and gray. Therefore, the bright and dark phase in part a are inverted in part b. Except for the inversion of the contrast, the two patterns (a) and (b) are essentially identical. In part a, we can observe a "double-wave structural unit" that appears bright, while in part b the corresponding unit appears dark, as shown in the inset of the each pattern. In other words, the matrix phase has the double-wave feature in both cases, though it appears bright in part a (unstained PS phase) and dark in part b (stained P2VP phase). One wave has large amplitude of oscillation, while the other wave has small amplitude of oscillation, both of which have a common wave vector **k**, as shown in the inset of part b. The set of the double wave is aligned periodically perpendicular to the wave vector **k**.

Close observations of the minority (PI) phase elucidate the following feature in both cases. The phase contains dark circles (part a) and bright circles (part b) periodically arranged along the wave vector **k**. The structural unit shown in the inset represents one repeat unit along the direction normal to the vector **k**.

It should be noted that the image in part a is somewhat distorted, probably due to deformation of the microdomain structure in the ultrathin-sectioning process. However, the distortion is much suppressed in the image of part b probably because the cross-linking of the matrix phase with DIB hardened the P2VP matrix and suppressed the distortion. Nevertheless a slight sliding deformation along the **k** vector is still discernible in the image of part b, as will be discussed in the next section.

III-2. Morphological Characterization of Ozone-Degraded Specimens with FE-SEM. While Figure 1 shows the TEM

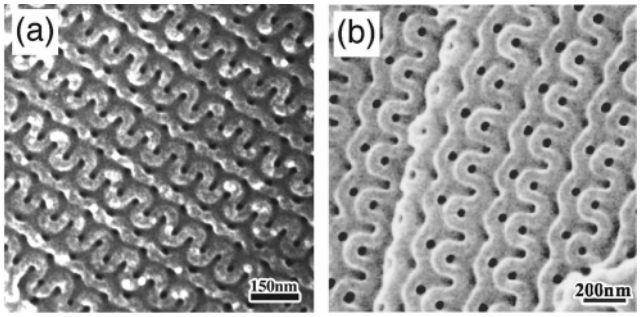

Figure 2. FE-SEM images representing the double-wave pattern on freeze−fractured surface of the ozone-degraded SI/HS films (a) and VI/HI films (b). In (b), the P2VP matrix was first cross-linked with 1,4-diiodobutane before the ozone degradation of the PI network phase.

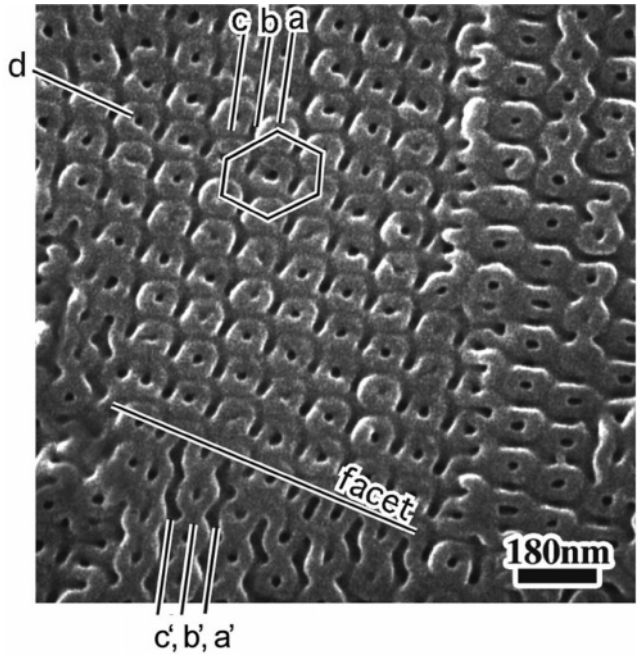

Figure 3. FE-SEM image, representing the hexagonal doughnut pattern with facets, on freeze−fractured surface of the ozone-degraded SI/HS films. Lines a, b, and c are shifted to the lines a′, b′, and c′ above and below the facet, respectively.

images, Figures 2 and 3 represent the most frequently observed FE-SEM images on the freeze-fractured surfaces for SI/HS (Figure 2a), VI/HI (Figure 2b), and SI/HS (Figure 3). Figure 2 shows the periodic double-wave patterns similar to that shown in the TEM images in Figure 1, while Figure 3 shows "doughnut-like patterns" arranged more or less in hexagonal symmetry. Some differences seen in the two images in Figure 2a,b may be due to those in the orientation of the fractured surface with respect to the electron beams or with respect to the crystallographic axes. The patterns shown in Figure 2a were dominant over the pattern shown in Figure 3.

It is important to note that the freeze−fracture may occur at planes parallel to particular crystallographic planes (called as cleavage planes) in the double-gyroid structure. Thus, FE-SEM studies may enable us to study cleaved surfaces of the structure. On the other hand, the ultrathin sectioning occurs more or less randomly with respect to the crystallographic planes. Therefore, TEM images themselves are a collection of those observed on the thin sections randomly cut with respect to the crystallographic axes. It is important to note that they are subjected to the effects of an overlap of the structure along the electron beam axis, though the effects do not exist on the SEM images.

IV. Numerical Analysis of FE-SEM Images and Discussion

IV-1. Method. We shall analyze the FE-SEM images presented in Figures 2 and 3 on the basis of the double-gyroid network structure. For this purpose we construct first computer graphics of various cross sections cut parallel to the particular crystallographic planes of the double-gyroid networks with given volume fractions of the network phase and then compare the computer graphics with the FE-SEM images.

The double-gyroid network was generated by applying the parallel surface method to the minimal surface of the gyroid that was given by the trigonometric approximation

$$f(x,y,z) = \sin\left(\frac{2\pi x}{L}\right)\cos\left(\frac{2\pi y}{L}\right) + \sin\left(\frac{2\pi y}{L}\right)\cos\left(\frac{2\pi z}{L}\right) + \sin\left(\frac{2\pi z}{L}\right)\cos\left(\frac{2\pi x}{L}\right) = 0 \quad (1)$$

Here L is the conventional unit cell edge length of the gyroid. The minimal surface given by eq 1 divides whole space into two subspaces with equal volumes, on both sides of which the double network was generated by applying the parallel surface method.[1]

IV-2. Numerical Analysis of FE-SEM Images. Figure 4 presents a skeletal model for the double gyroid (part a) as well as the computer graphics of the unit cell of the structure in which the network phase is made empty (part b) and 3D cross section of network cut parallel to (211) plane at a particular point ($x_0 = 0.5$ as will be defined later) in the crystal unit cell (part c). In Figure 4a the double-gyroid network is seen to be comprised of two sets of the red and blue networks intertwined one another without touching, and each network in turn is made by regularly connected structural unit of the special tripods in 3D space. In

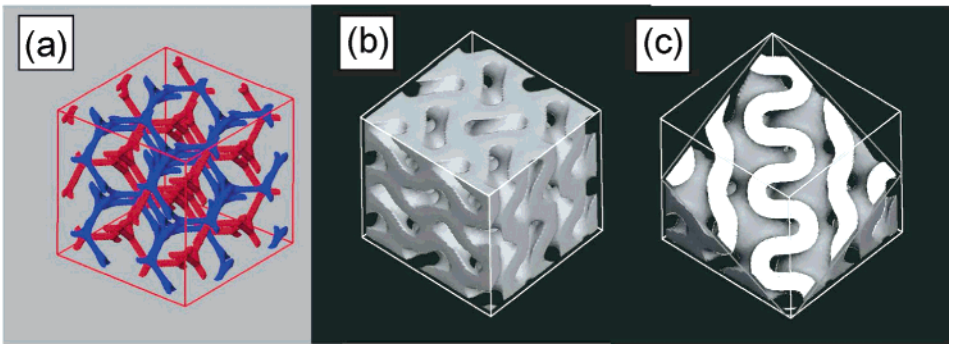

Figure 4. Computer graphics for a unit cell of the double-gyroid network system with $Ia\bar{3}d$ space group symmetry: (a) skeletal model, (b) the cell in which the double-network phase is made empty and the matrix phase is represented by gray, and (c) a cross-sectional view cut at a particular plane parallel to (211) plane.

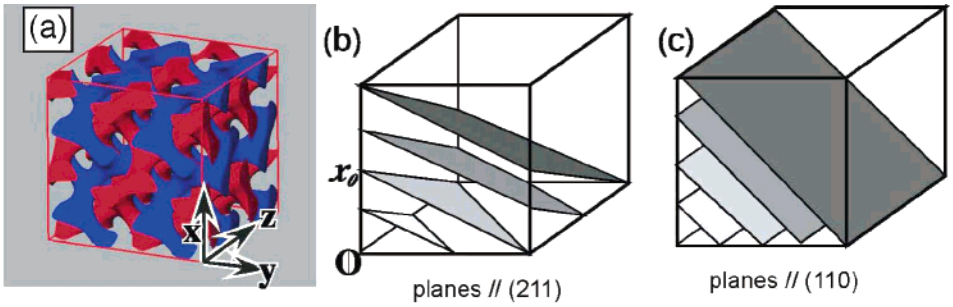

Figure 5. (a) Definition of the origin of the *xyz* coordinate with respect to the double-gyroid network structure. Definitions of a series of planes cut parallel to particular crystallographic planes, e.g., (211) plane (b) and (110) plane (c).

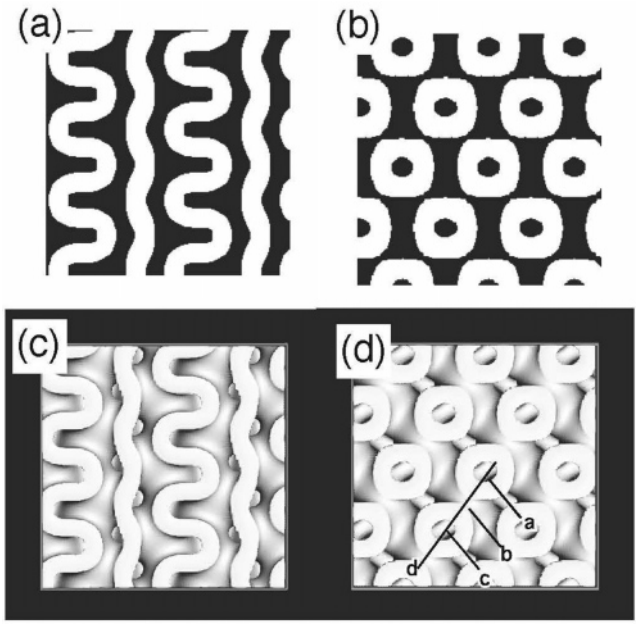

Figure 6. Computer graphics of cross-sectional images of the double-gyroid network cut parallel to (211) plane (parts a and c) at $x_0 = 0$, 0.5, 1.0, etc., and (110) plane (parts b and d) at $x_0 = 0$, 0.25, 0.5, 0.75, 1.0, etc. Parts a and b correspond to 2D images of the cross sections, while parts c and d correspond to 3D images of the cross sections.

Figure 4b, the matrix phase and the two sets of the vacant channel corresponding to the double-gyroid networks were presented as gray phase and empty phase, respectively. This figure shows cross-sectional view cut parallel to (100), (010), and (001) planes as well. In the cross section shown in Figure 4c the matrix phase and the vacant channel (or network) were presented bright and gray in order to facilitate a comparison with the FE-SEM images shown in Figure 2. It is obvious that the computer-constructed cross section in Figure 4c represents well the double-wave pattern of the observed FE-SEM image shown in Figure 2a.

Figure 5 defines the position of a cross-sectional plane cut parallel to a particular crystallographic plane (*hkl*). The plane is defined by

$$h(x - x_0) + ky + lz = 0 \qquad (2)$$

where x_0 is the position of the cross section which is reduced with respect to the length of the cell edge ($0 \le x_0 \le 1$). Part a represents the Cartesian coordinate for the double-gyroid network structure, while parts b and c represent respectively a series of the cross sections parallel to the (211) plane with $h = 2$, $k = 1$, and $l = 1$ and the (110) plane with $h = k = 1$, $l = 0$ with $0 \le x_0 \le 1$.

Figure 6 represents computer graphics on the cross-sectional images of the double-gyroid network in which the vacant double network channel phase is shown either dark (in parts a and b) or gray (in parts c and d), and the matrix phase is shown bright. Parts a and b represent 2D images of the cross sections parallel to (211) at $x_0 = 0.5$ and to (110) at $x_0 = 0.25$ planes, respectively, while parts c and d represent 3D images of the corresponding cross sections of parts a and b, respectively. The 2D images in parts a and b qualitatively represent respectively the characteristics of the double-wave pattern and the hexagonal doughnut pattern found in the experimental images shown in Figures 2a and 3. The 3D images in parts c and d quantitatively represent respectively the characteristics of the double-wave pattern and the hexagonal doughnut pattern found in the experimental images even with respect to the contrast variation of the gray phase. Since FE-SEM captures topographical characteristics of the freeze-fractured surface, its image can be better represented by the computer graphics on the 3d cross-sectional images. In the graphics the dent region is shown by gray to dark depending on the depth of the dent relative to the bright and flat matrix area.

The 3D cross-sectional image in Figure 6c reproduces a series of circles along both the large-amplitude waves and the small-amplitude waves parallel to the **k** vector as observed in Figure 1 and Figure 2a, though the circles along the large-amplitude waves are less distinct than those along the small-amplitude waves. We believe that a slight tilting of the cross section will make them clearer. A close comparison of Figures 1b and 6c indicates that the TEM image in Figure 1b reveals a sliding deformation of a set of the large- and small-amplitude waves along the **k** vector relative to the neighboring sets by about one-half of the spacing. However, the sliding deformation shown in the FE-SEM image in Figure 2a is much less than that in Figure 1b. Thus, the freeze−fracturing appears to involve less deformation than the ultramicrotoming. This is quite intriguing from the viewpoint of micromechanics of the nanomaterials. The 3D cross-sectional image in Figure 6d reproduces topographic difference along the line a (or b) and line d in Figure 3: along the line d we observe a dent between successive doughnut, while along the line a or b we do not observe the dent. The line d in Figure 3 corresponds to the line d in Figure 6d, while the lines a and c in Figure 3 correspond to the lines a and c in Figure 6d, respectively. The difference of the pattern along line a and line d which can be seen in the 3D cross-sectional image in part d cannot be detected in the 2D cross-sectional image in part b. Thus, the 3D cross-section image gives more information than the 2D one.

IV-3. Analysis of Cleavage Planes of Materials Having the Voided Double-Gyroid-Channel Morphology. The area fraction of the matrix phase $S(x_0)$ which appeared on the 2D cross-sectional image obtained by cutting the double-gyroid

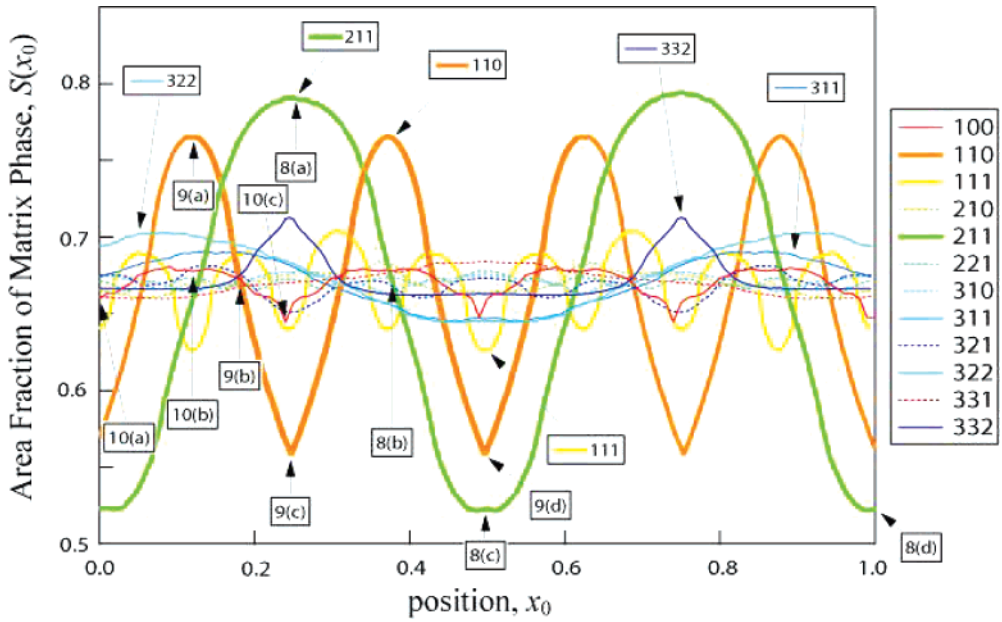

Figure 7. Calculated area fraction of the matrix phase $S(x_0)$ cut along the planes parallel to various crystallographic planes, as shown by three digits *hkl* in the legend, at various positions x_0. The arrows labeled by 8(a) to 8(c), 9(a) to 9(c), and 10(a) to 10(c) represent the positions where their cross-sectional images are demonstrated, respectively, in Figures 8a−c, 9a−c, and 10a−c.

network structure parallel to various crystallographic planes (*hkl*) was estimated as a function of the position x_0. The results are shown in Figure 7, where $S(x_0)$ is plotted against x_0 for various crystallographic planes. The value $S(x_0)$ varies remarkably with x_0 around the mean value of 0.66 only for the planes parallel to (211) (green) and (110) planes (brown), while the value hardly depends on x_0 but is rather constant nearly equal to 0.66 for other crystallographic planes such as (210), (221), and (310), though a slightly larger position dependence is seen for (100), (111), (311), (321), (322), (331), and (332). For the cross section parallel to the (211) plane, the values $S(x_0)$ become a minimum value of 0.525 at $x_0 = 0$, 0.5, 1.0, etc., and a maximum value of 0.79 at $x_0 = 0.25$, 0.75, etc. Thus, the planes at $x_0 = 0$, 0.5, 1.0, etc., are anticipated to be the cleavage planes parallel to (211) plane. On the other hand, for the cross section parallel to (110) plane, the values $S(x_0)$ become a minimum value of 0.55 at $x_0 = 0$, 0.25, 0.5, 0.75, 1.0, etc., and a maximum value of 0.77 at $x_0 = 0.125$, 0.375, 0.625, 0.875, etc. Thus, the planes at $x_0 = 0$, 0.25, 0.5, 0.75, 1.0, etc., are anticipated to be the cleavage plane parallel to (110).

The cross-sectional images with the minimal cross-sectional area parallel to (211) plane are shown in Figure 6a,c and that parallel to (110) plane in Figure 6b,d. In fact, we found most frequently the image on the cleavage plane parallel to (211) plane and the image on the cleavage plane parallel to (110) plane with a lower frequency. These pieces of evidence are quite reasonable with respect to the difference in the minimum values of $S(x_0)$ between the two cases. Figure 8 shows a series of 2D cross-sectional images, on the planes cut parallel to (211) plane at $x_0 = 0.25$ (a), 0.375 (b), and 0.5 (c), and the corresponding 3D cross-sectional images are shown in (d) to (f), respectively. On the other hand, Figure 9 shows a series of 2D cross-sectional images on the planes cut parallel to (110) plane at $x_0 = 0.125$ (a), 0.1875 (b), and 0.250 (c) and the corresponding 3D cross-sectional images are shown in (d) to (f), respectively. In both cases the change of $S(x_0)$ with x_0 is quite obvious. The lines (a) to (c) in Figure 9f correspond to those in Figure 3 and in Figure 6d.

Figure 10 shows examples of the series of 2D cross-sectional images cut parallel to the crystallographic planes which do not have appreciable changes in $S(x_0)$ with x_0, one for the planes parallel to (100) plane, as a typical example of planes having relatively low indices, at $x_0 = 0.0$ (part a), 0.125 (part b), and 0.25 (part c) and the other for the planes (322) (part d), (421) (part e), and (432) (part f), as examples of planes having relatively high indices, at $x_0 = 0$. The patterns are different, but the area fraction is almost the same.

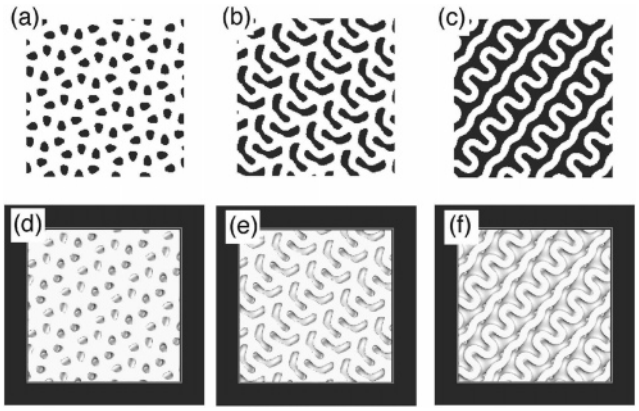

Figure 8. Computer graphics of the 2D (parts a to c) and 3D (parts d to f) cross-sectional images of the double-gyroid network cut along the plane parallel to (211) plane at the three positions: $x_0 = 0.25$ (parts a and d), $x_0 = 0.375$ (parts b and e), and $x_0 = 0.5$ (parts c and f).

IV-4. Analysis of Facets Observed in Cleavage Surfaces. Figure 11 represents typical facets observed in FE-SEM images on the freeze-fractured surface. The facet seems to have the following characteristics. (i) The double-wave pattern is slightly shifted across the facet in such a way that the center line of the wave of a large (small)-amplitude oscillation appears to be connected to the center line of the wave of a small (large)-amplitude oscillation, as schematically shown in the inset for example. (ii) The two surfaces across the facet seem to have a definite step height. (iii) The facet seems to have a definite angle with respect to the center line of the wave, although the angle appears to vary somewhat in Figure 11 due to the distortion of the structure in the freeze−fracture process.

We analyzed the facet below on the basis of the assumption that the two surfaces on both sides of the facet correspond to

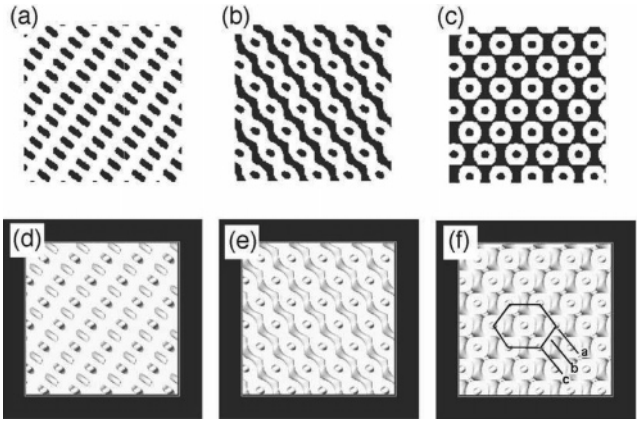

Figure 9. Computer graphics of the 2D (parts a to c) and 3D (parts d to f) cross-sectional images of the double-gyroid network cut along the plane parallel to (110) plane at the three positions: $x_0 = 0.125$ (parts a and d), $x_0 = 0.1875$ (parts b and e), and $x_0 = 0.25$ (parts c and f).

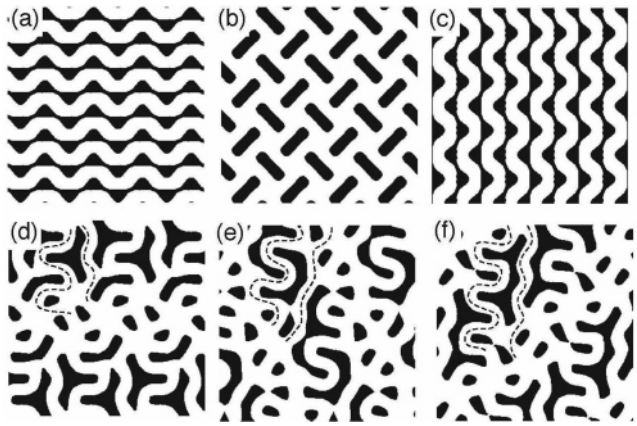

Figure 10. Computer graphics for a series of the 2D cross-sectional images cut along the plane parallel to the crystallographic planes at various positions x_0 for the case in which $S(x_0)$ does not change appreciably with x_0. Parts a to c show the images on the planes cut parallel to (100) plane at $x_0 = 0$, 0.125, and 0.25, respectively, representing the planes having relatively low Miller indices. Parts d to f show the images on the planes parallel to (322), (421), and (432) at $x_0 = 0$, respectively, representing planes having relatively large Miller indices.

the surfaces having the minimum matrix cross-sectional area (0.53), cleaved at $x_0 = 0$ and 0.50, as estimated in Figure 7, with a step-height difference h_s equal to Δx_0 ($\mathbf{n}\cdot\mathbf{n}_x$) = 0.41 where $\Delta x_0 = 0.5$, the reduced distance between the two successive cross-section points of the planes parallel to (211) plane having the minimum cross-sectional area; $\mathbf{n}$ and $\mathbf{n}_x$ are unit vectors parallel to the reciprocal lattice vector of (211) plane and to x-axis, respectively. On the basis of this assumption, we tried to reproduce the facet shown in Figure 11 by computer graphics. The results are presented in Figure 12.

Figure 12 represents computer graphics of 3D cross-sectional images, viewed from top (part a) and slightly inclined view relative to part a (part b), both of which have a facet having the step height h_s running from bottom-left to top-right with a specific orientation angle of 65° arc with respect to the center line of the double-wave pattern. Figure 12c shows the 3D cross-sectional image viewed from the edge direction of Figure 12b, as shown by the arrow in Figure 12b. The arrow in part b corresponds to that in part c. The computer graphics in Figure 12c facilitate the observation of the facet and the step height between the two cleavage surfaces represented by Figure 12a,b. Moreover, Figure 12d shows the pattern on the plane which

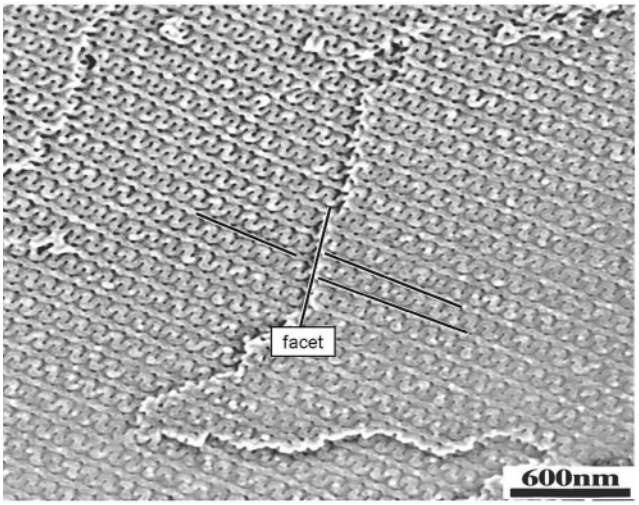

Figure 11. FE-SEM image showing facets observed for the cleavage surface parallel to (211) plane on the freeze−fractured SI/HS films subjected to the ozone degradation.

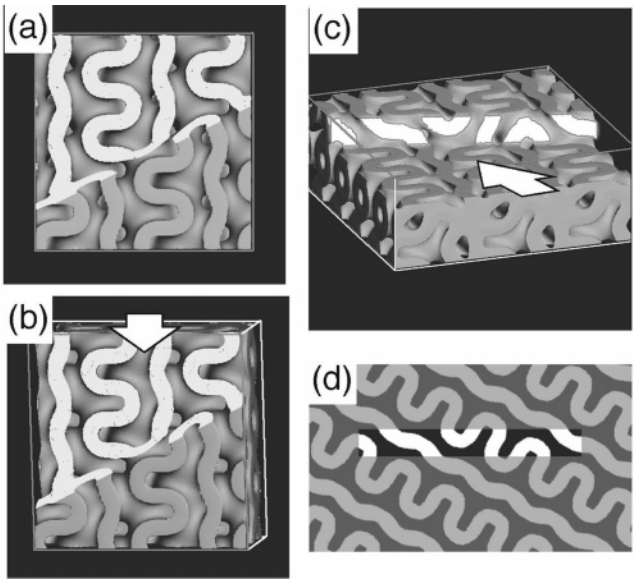

Figure 12. Computer graphics showing the facet with a step height of proportional to $\Delta x_0 = 0.5$ (see the text in detail) created on the cleavage surface parallel to (211) plane. Part a shows the 3D cross-sectional image of the cleaved surface viewed from the top (part a), while part b shows that viewed from a slightly inclined direction with respect to the surface normal. Part c shows the facet viewed from an edge shown by the arrow in (b); the two arrows in parts b and c correspond to each other. Part d shows the pattern on the plane which includes the facet and which is normal to the plane showing the double wave pattern in parts b and c. The central portion in part d distinguished by a different contrast with its surrounding corresponds to the portion of the step shown in part c.

includes the facet and which is normal to the plane showing the double-wave pattern in parts b and c. It reveals that the facet itself may correspond to the cleavage plane having the double-wave pattern and hence the minimum cross-sectional area parallel to (211) plane. The central part in Figure 12d represented by a different contrast against its neighbor corresponds to the vertical step seen in Figure 12c. The computer graphics shown in Figure 12a,b successfully capture, at least qualitatively, the features i to iii found for the experimental facet image. Furthermore, the graphics shown in Figure 12c,d elucidate that the facet occurs also along the (211) cleavage plane.

We can discern the facet on the cleavage plane parallel to (110) plane, too. An example was shown by the line labeled

facet drawn on the image in Figure 3. Lines a to c are seen to be shifted to the lines a′ to c′ across the facet, respectively.

V. Conclusion

We unequivocally identified the "voided double-gyroid-channel" morphology which was fabricated from the double-gyroid cubic structure by transforming the network phase into the vacant phase. We elucidated that the new morphology, which keeps the cubic structure with $Ia\bar{3}d$ symmetry and is potentially important for nanotechnology, has two cleavage planes on which the cross-sectional area of the morphology becomes minimal.

References and Notes

(1) See for example: Hyde, S.; Andersson, S.; Larsson, K.; Blum, Z.; Landth, T.; Lidin, S.; Ninham, B. W. *The Language of Shape*; Elsevier: Amsterdam, 1997.
(2) See for example: Hamley, I. *The Physics of Block Copolymers*; Oxford University Press: Oxford, 1988.
(3) Kaneda, M.; Tsubakiyama, T.; Carlsson, A.; Sakamoto, Y.; Ohsuna, T.; Terasaki, O.; Joo, S. H.; Ryoo, R. *J. Phys. Chem. B* **2002**, *106*, 1256.
(4) Luzzati, V.; Tardieu, A.; Gulik-Krzywicki, T.; Rivas, E.; Reiss-Husson, F. *Nature (London)* **1968**, *220*, 285.
(5) Seddon, J. M. *Biochim. Biophys. Acta* **1990**, *1031*, 1.
(6) Khandpur, A. K.; Förster, S.; Bates, F.; Hamley, I. W.; Ryan, A. J.; Bras, W.; Amdal, K.; Mortensen, K. *Macromolecules* **1995**, *28*, 8796.
(7) Hajduk, V. A.; Harper, P. E.; Gruner, S. M.; Honeker, C. C.; Kim, G.; Thomas, E. L.; Fetters, L. J. *Macromolecules* **1994**, *27*, 4063.
(8) Jinnai, H.; Nishikawa, Y.; Spontak, R. J.; Smith, S. D.; Agard, D. A.; Hashimoto, T. *Phys. Rev. Lett.* **2000**, *84*, 518.
(9) Hajduk, D. A.; Harper, P. E.; Gruner, S. M.; Honeker, C. C.; Thomas, E. L.; Fetters, L. J. *Macromolecules* **1995**, *28*, 2570.
(10) Zhao, J.; Majumdar, B.; Schulz, M. F.; Bates, F.; Almdal, K.; Mortensen, K.; Hajduk, D. A.; Gruner, S. M. *Macromolecules* **1996**, *29*, 1204.
(11) Hashimoto, T.; Tsutsumi, K.; Funaki, Y. *Langmuir* **1997**, *13*, 6869.
(12) Tsutsumi, K.; Funaki, Y.; Hirokawa, Y.; Hashimoto, T. *Langmuir* **1999**, *15*, 5200.
(13) Okumura, A.; Nishikawa, Y.; Hashimoto, T. *Polymer* **2006**, *47*, 7805.
(14) Lee, J. S.; Hirao, A.; Nakahama, S. *Macromolecules* **1988**, *21*, 276.
(15) Barnes, I. S.; Hyde, S. T.; Ninham, B. W. *J. Phys., Colloq.* **1990**, supplement to *51*, C7-19.

MA061739H